Journal of Computational Design and Engineering, Vol. 1, No. 1 (2014) 13~26
www.jcde.org

As-built modeling of piping system from terrestrial laser-scanned point clouds using normal-based region growing

Kazuaki Kawashima*, Satoshi Kanai and Hiroaki Date
Graduate School of Information Science and Technology, Hokkaido University, Sapporo, Japan

(Manuscript Received September 18, 2013; Revised October 26, 2013; Accepted November 1, 2013)

Abstract

Recently, renovations of plant equipment have been more frequent because of the shortened lifespans of the products, and as-built models from large-scale laser-scanned data is expected to streamline rebuilding processes. However, the laser-scanned data of an existing plant has an enormous amount of points, captures intricate objects, and includes a high noise level, so the manual reconstruction of a 3D model is very time-consuming and costly. Among plant equipment, piping systems account for the greatest proportion. Therefore, the purpose of this research was to propose an algorithm which could automatically recognize a piping system from the terrestrial laser-scanned data of plant equipment. The straight portion of pipes, connecting parts, and connection relationship of the piping system can be recognized in this algorithm. Normal-based region growing and cylinder surface fitting can extract all possible locations of pipes, including straight pipes, elbows, and junctions. Tracing the axes of a piping system enables the recognition of the positions of these elements and their connection relationship. Using only point clouds, the recognition algorithm can be performed in a fully automatic way. The algorithm was applied to large-scale scanned data of an oil rig and a chemical plant. Recognition rates of about 86%, 88%, and 71% were achieved straight pipes, elbows, and junctions, respectively.

Keywords: Laser scanning; Object recognition; As-built model; Piping system; Point clouds

1. Introduction

Recently, because of the short lifespans of plant products, renovations of plant equipment have been more frequent. However, the results of the renovations are not necessarily recorded in the plant drawings in many cases. Thus, unintended collisions between existing equipment and newly designed ones often take place in the construction stage. This causes additional costs and labor.

The performance of terrestrial laser scanners has been rapidly developing, and shapes of objects in environments can be easily captured as 3D point clouds. With these laser-scanned point clouds of existing plants, an as-built model of the plant equipment could be reconstructed. Once the model is reconstructed, the unintended works could be pre-checked on computers and avoided in the planning stage.

However, the laser-scanned data of existing plants have massive point clouds, include a large amount of noise, and capture tangled objects. Therefore, recognizing each plant component from the point cloud, including the tangled objects, and constructing a 3D model of the plants are nearly impossible or very time-consuming when done in an interactive way. Thus, automation of the recognition and 3D model construction processes from point clouds need to be strongly promoted in the plant engineering field.

Plants consist of many types of components. One of the more important components is a piping system, which accounts for the greatest proportion and is renovated frequently. A piping system consists of various elements and their connection relationships: straight pipes, connecting parts such as junctions and elbows, and attached parts such as indicators and valves.

Several studies have been proposed to recognize piping systems from laser-scanned point clouds. However, these algorithms cannot be applied to the point clouds that have already been registered and the intensity, or that can only recognize few classes of piping systems. Masuda et al. [1] proposed a method which could recognize planes and cylinders from the scanned data of plants. However, it required the combination of a scanned point and reflected intensity from a scanner. Rabbaini et al. [2] proposed a method that reconstructed a 3D primitive model from the combination of a point cloud and a photograph taken from the same location. However, the method needed a pair of point cloud data and a photo shot from the scanner position. Piping systems often occupy a broad area of plants, and multiple scans and their

*Corresponding author. Tel.: +82-011-706-6449, Fax.: +82-011-706-7120
E-mail address: k_kawashima@sdm.ssi.ist.hokudai.ac.jp

doi: 10.7315/JCDE.2014.002

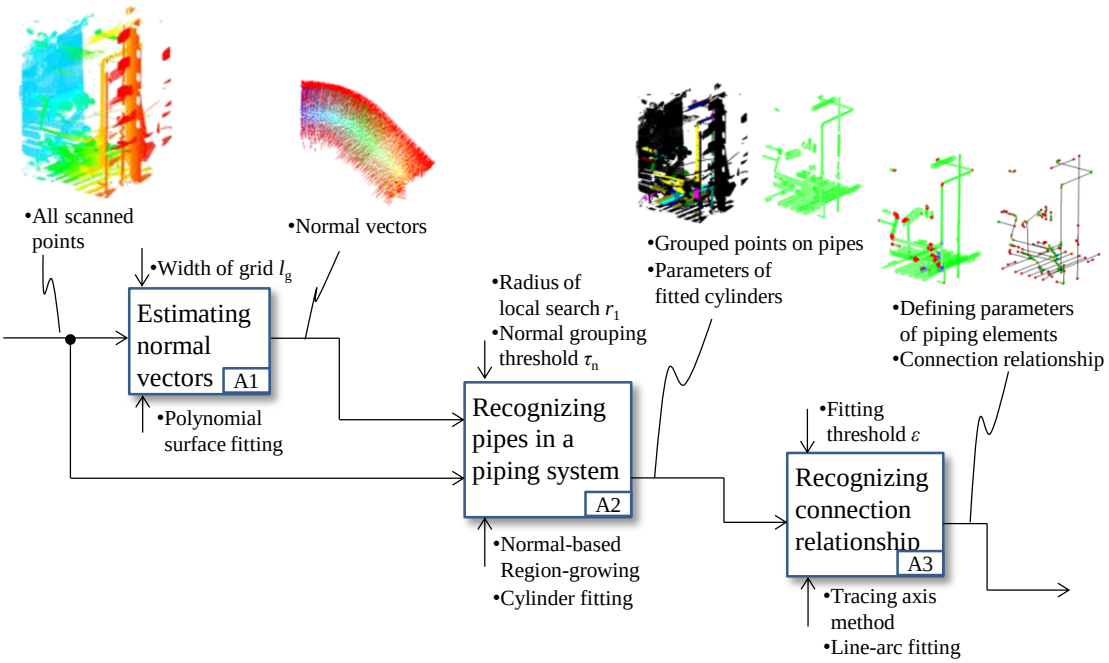

Figure 1. The overview of the proposed piping system recognition algorithm.

registration are inevitable to obtain a point cloud covering the whole shape of the system. Therefore, it is probable that these algorithms cannot be applied to a registered point cloud generated from multiple scans. Aurelien et al. [3] proposed a method which fits an optimized cylinder model to the scanned points using an a priori CAD model of plants. However, 3D cylinder models, which have similar radii and axis directions, have to be placed near the points on pipes manually. Johnson et al. [4] proposed a method which matches a 3D CAD model in a database to a point cloud using a spin image. However, it is difficult to prepare an exact 3D model of straight pipes because their lengths are not fixed. Namatame et al. [5] proposed a method which recognized points on pipes under the assumption of Manhattan World Grammar. However, the algorithm could only recognize the straight portion of a piping system. Recently, Lee et al. [6] proposed a method which recognized straight pipes, elbows, and junctions from points on a piping system using the voronoi diagram. However, in their algorithm, the input point cloud only included the pipes themselves, and did not include any unwanted parts, such as flanges or valves, or supporting members, thus sacrificing generality. Belton et al. [7] and Rabbani et al. [8] proposed methods that classified and partitioned the scanned points of plants into those on planar surfaces and on cylindrical surfaces using covariance analysis and using a combination of normal-based region growing and plane fitting. However, points on elbows and junctions and the connectivity of the piping systems were not identified. Vosselman et al. [9] proposed a method using 3D Hough transforms for recognition. However, only straight pipes are recognized in the piping system. El-Harawany et al. [10] proposed a method that identified cylinders from scanned points of pole-like objects on a road side using a combination of eigen-based segmentation, linear feature extraction, and cylinder fitting. However, if applied to scanned points of plants, only straight pipes could be extracted from them. Marshall et al. [11] proposed a non-linear least-square-based method where scanned points of general objects are segmented into spheres, cylinders, cones, and tori. However, the method dealt only with the point clouds of relatively simple-shaped objects, so it could not work well when applied to the tangled objects in plants.

Therefore, the purpose of this research was to propose a new algorithm that could automatically recognize piping elements consisting of straight pipes and connecting parts and their connection relationships only from raw laser-scanned point clouds of a whole plant, which includes point clouds other than the piping system. The algorithm was tested for large-scale laser-scanned point clouds of a real plant, and the recognition accuracy of the straight pipes and connecting parts were verified.

We have already proposed a similar recognition algorithm of piping systems, but it had some problems [12]. In the process of extracting points on straight pipes, a delicate parameter setting of the searching radius was needed. The parameter should be set in relation to a pipe radius on which the point lies. Therefore, if there is a great distinction among the radii of pipes in the plant, then most of the pipes cannot be extracted. Moreover, the algorithm could not extract some points around non-straight pipes such as supporting materials, attached parts, and junction parts on a straight pipe. Therefore, if tangled pipes are concentrated in a small area, these pipes would not be recognized.

To solve these problems, this paper introduces a normal-

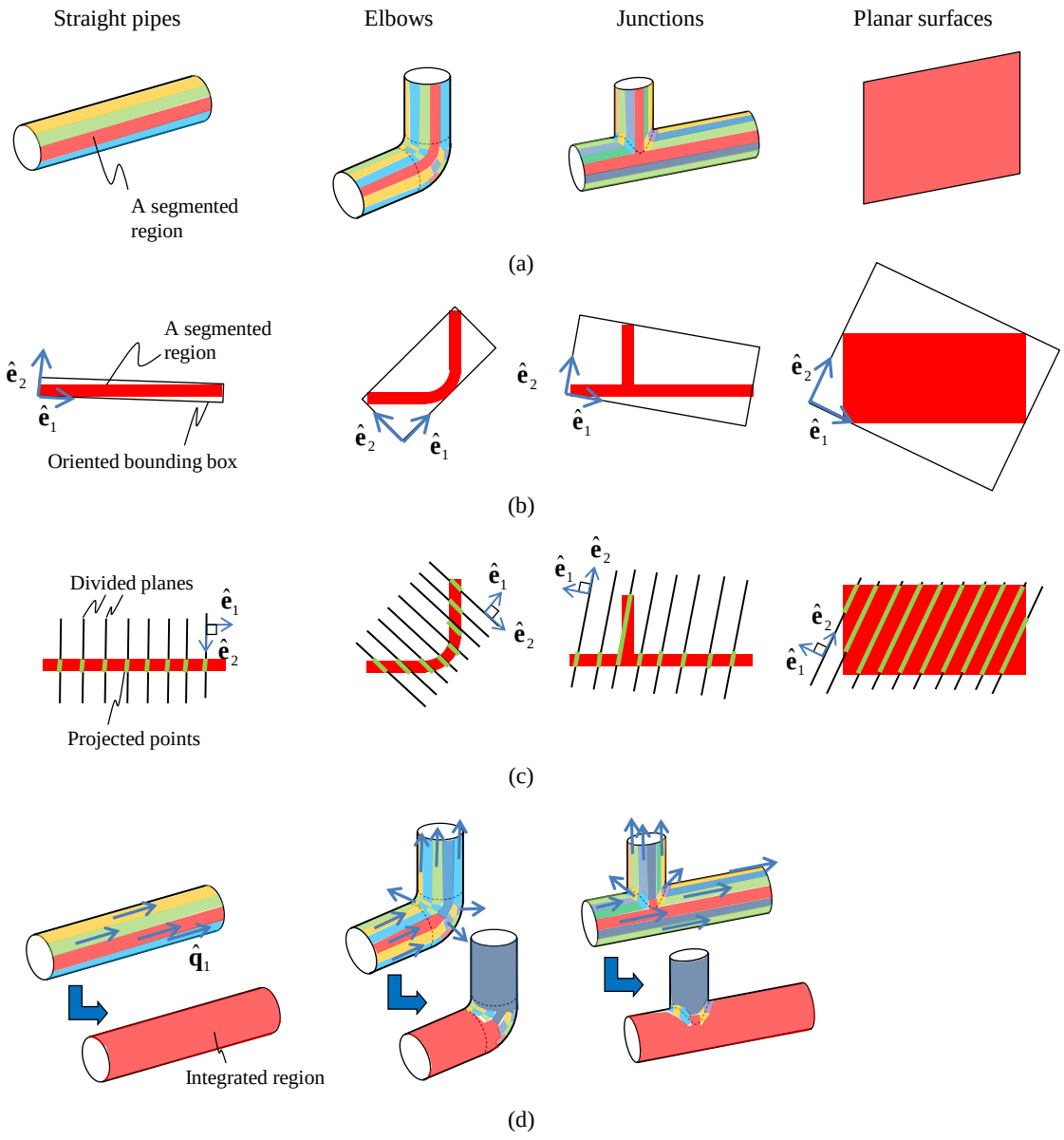

Figure 2. Recognizing pipes of a piping system: (a) normal-base region growing, (b) oriented bounding box, (c) median of ranges of projected points, (d) integrated region.

based region growing which automates the extraction of points on a piping system and segmentation of points into each pipe. By introducing the algorithm, almost all points of pipes can be extracted without calculating the normal tensor. With this method, great improvement was achieved in the recognition rates of straight pipes, junctions, and elbows than with previous methods [12].

2. Algorithm overview

As shown in Figure 1, the proposed recognition algorithm consists of three processes. First, the normal vector of every scanned point is estimated using grid cells and quadratic polynomial surface fitting. Next, the points on each pipe are extracted using normal-based region growing, and their radii and positions are estimated by cylindrical surface fitting. Finally, the connection relationships among the extracted pipes are recognized by tracing and interpolating axes of the recognized pipes.

3. Estimating normal vectors

In order to reduce computational costs of normal vectors for a huge set of scanned points, a grid whose cell has a width l_g is placed to cover the whole scanned space. Each grid cell keeps scanned points inside the cell. In the algorithm,

l_g is recommended to be set as one third of the smallest pipe radius r_{min} to be dealt with in the piping system.

Next, in order to estimate the normal vectors of all scanned points, for each grid cell i, the covariance matrix C_i is first calculated by equation (1).

$$C_i = \frac{1}{|\{\mathrm{p}_j\}|}\sum_{j=1}^{|\{p_j\}|}\left(\mathrm{p}_j - \mathrm{b}_i\right)^T\left(\mathrm{p}_j - \mathrm{b}_i\right) \quad (1)$$

where $\{\mathrm{p}_j\}$ is a set of position vectors of the points inside the cell i and its one-neighboring 26 grid cells, and b_i is an average position vector of $\{\mathrm{p}_j\}$. The eigenvalues $\lambda_1\lambda_2\lambda_3(\lambda_1 \geq \lambda_2 \geq \lambda_3 \geq 0)$and corresponding eigenvectors e_1, e_2, e_3 are obtained by an eigenvalue analysis of C_i. If $l_\sigma$is sufficiently smaller than the radius of the pipe, the points $\{\mathrm{p}_j\}$ are approximately distributed on a plane, and the eigenvectors e_1 and $e_2$indicate the principal axes placed on the plane. Therefore, the vector e_3 approximates the normal vectors at all points $\{\mathrm{p}_j\}$. Thus, e_3 is adopted as an initial normal vector n_i'. Next, a local orthogonal coordinate system $\mathrm{u}-\mathrm{v}-\mathrm{w}$ whose origin is placed at b_i with $u//e_1$, $\mathrm{u}//e_2$, and $\mathrm{w}//n_i'$ is selected. Then, $\{\mathrm{p}_j\}$ are projected onto the plane $\mathrm{u}-\mathrm{v}$. An explicit quadratic polynomial surface $\mathrm{w} = \mathrm{h}(u,v)$ of equation (2) is then fitted to $\{\mathrm{p}_j\}$ using the least squares method.

$$\mathrm{w} = \mathrm{h}(u,v) = a_o u^2 + a_1 u^2 + a_2 uv + a_3 u + a_4 v + a_5 \quad (2)$$

Finally, $\{\mathrm{p}_j\}$ are projected onto the surface to obtain their projected points $\{\mathrm{p'}_j\}$, and the normal vector of $\mathrm{w} = \mathrm{h}(u,v)$ at every projected point p_i' in the original coordinate frame (x,y,z) is estimated as a normal vector n_i of p_i.

4. Recognizing pipes in a piping system

4.1 Extracting points on a piping system

In order to extract points on a piping system from all scanned points P, a normal-based region growing was developed. First, the normal-based region growing is applied. In the region growing, a seed point $p_s \in P$ is chosen from P at random. Then, the points $\{\mathrm{p}_i|\mathrm{p}_i \in P, \mathrm{p}_i \in N(\mathrm{p}_s, r_1), \|\mathrm{n}_s \cdot \mathrm{n}_i\| > \tau_n\}$ are extracted and added to a region, where $N(\mathrm{p}_s, r_1)$is a set of neighboring scanned points contained in the sphere of the radius $r_1$centered at p_s. The threshold $\tau_n$was set to 0.97 based on our experiments. Each of the added points is then chosen as a new seed point, and the other points satisfying the same condition are progressively added to the region. These steps are iterated until any points satisfying the condition exist in the neighborhood of the seed points.

After the region-growing process, a covariance matrix is calculated for all points in every region $\{\mathrm{p}_j\}$, and eigenvalues $\hat{\lambda}_1, \hat{\lambda}_2, \hat{\lambda}_3\left(\hat{\lambda}_1 \geq \hat{\lambda}_2 \geq \hat{\lambda}_3 \geq 0\right)$ and corresponding eigenvectors $\hat{e}_1, \hat{e}_2, \hat{e}_3$ are obtained. An oriented bounding box which aligns to the vectors $\hat{\mathbf{e}}_1, \hat{\mathbf{e}}_2, \hat{\mathbf{e}}_3$ is fit to the points $\{\mathbf{p}_n\}$. As shown in Figure 2(a) and Figure 2(b), if the scanned points exist on straight pipes, the regions take the shape of thin strips placed along the pipe axis, and the vector $\hat{\mathbf{e}}_1$ approximates the axis direction of the pipe. If the points exist on elbows or junctions, the region takes the concatenated shape of thin straight strips and thin circular strips. In contrast, if the points exist on wide planar surfaces such as floors or walls, the region takes the shape of a broad width.

Then, as shown in Figure 2(c), several numbers of dividing planes whose normal vectors are equal to $\hat{\mathbf{e}}_1$ are placed at regular intervals, and the points in $\{\mathbf{p}_n\}$ are projected onto the nearest plane. Moreover, on each plane, the set of the projected points is further projected onto the line parallel to $\hat{\mathbf{e}}_2$, and the range of the projected points on the line is evaluated. If the median value of the ranges $\hat{d}$ satisfy $\hat{d} < \tau_w$, where τ_w is a threshold, the regions are classified as points on the piping system, such as straight pipes, elbows, and junctions. Otherwise, they are classified as points on the other components, such as planar surfaces. As for the threshold, τ_w was set as $2.0 \cdot r_{max} \sin\cos^{-1}(\tau_n)$ from a simple geometric relation, where r_{max} is the radius of the largest pipe in the measured environment.

For parts of regions on elbows or junctions, the vector $\hat{\mathbf{e}}_1$ is not coincident with the axes vectors of the pipes. Therefore, to modify the segmentation, a line is fitted to each region using RANSAC. The number of sampling in the RANSAC is set as 50, and the outlier threshold to the distance between a point in the region and the fitted line is set as $\hat{d}/2.0$.

Finally, the points whose distance to the fitted line was less than the outlier threshold were chosen and segmented as one region. The remaining points will be segmented iteratively using the above region-growing process.

4.2 Grouping points on a pipe segment

In order to integrate the segmented regions into a new single region which belong to a same pipe, the constraint region-growing is further applied to points on the piping system.

First, as shown in Figure 2(d), a covariance matrix E is calculated for the set of points in a region, and the eigenvector $\hat{\mathrm{q}}_1$corresponding to the largest eigenvalue of E is assigned to all scanned points in the region.

Next, a seed point $\mathbf{p}_s$ is chosen from the points on a piping system at random. Then, the other points $\mathbf{p}_i$ which satisfy $\left\|\hat{\mathbf{q}}_{1,s} \cdot \hat{\mathbf{q}}_{1,i}\right\| > \tau_q$ contained in neighboring points $\mathrm{N}(\mathbf{p}_s, r_1)$ centered at p_s are added into the region. τ_q was set to be 0.95 based on our experiments. Each of the added points is next chosen as a new seed point.

The above steps are iterated until any points satisfying the condition appear in the neighborhood of the seed points.

4.3 Extracting the pipe parameters

After grouping points on the pipe segments, a cylinder is

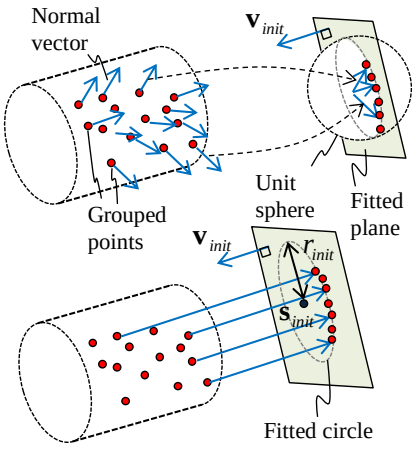

Figure 3. Initial cylinder fitting.

fitted to each pipe region, and the axis of the pipe and its radius are estimated.

As shown in Figure 3, for each region, normal vectors of the grouped points are first projected to a unit sphere surface. Then, a plane is fitted to the projected normal vectors using RANSAC, and the normal vector of the plane is determined as an initial axis vector of the cylinder v_{init}. The number of sampling in the RANSAC is set as 50, and the outlier threshold to the inner product of normal vectors is set as 0.01. Then, all points in the region are projected onto the fitted plane, and a circle is fitted to the projected points by the Least Median of Squares (LMedS) [13].

The number of sampling in the LMedS is set as 50. The center point and the radius of the circle are determined as the point on the axis s_{init} and the initial radius r_{init} of the cylinder.

Next, a cylinder is precisely fitted onto the points by the Levenberg-Marquardt method [14]. In this method, parameters of a cylinder model are expressed as seven variables $(\alpha, \beta, \gamma, a, b, c, r)$, where (α, β, γ) is the unit axis vector of the cylinder, (a, b, c) is the point coordinates on the axis, and r is the cylinder radius. Finally, an objective function of the cylinder fitting is expressed as equations (3), (4), and (5).

$$\frac{1}{N}\sum_{i=0}^{N-1}(f_i - r)^2 \rightarrow \min \tag{3}$$

$$f_i = \sqrt{m^2 + n^2 + o^2} \tag{4}$$

$$\begin{aligned} m &= \gamma(y_j - b) - \beta(z_i - c) \\ \mathrm{n} &= \alpha(z_i - c) - \gamma(x_i - a) \\ \mathrm{o} &= \beta(x_i - a) - \alpha(y_i - b) \end{aligned} \tag{5}$$

where (x_i, y_i, z_i) is a position vector of the grouped point. Then, based on the obtained radii r from equation (3), outlier points which satisfy $(r < r_{min}) \vee (r > r_{max})$ are removed from the points on the piping system.

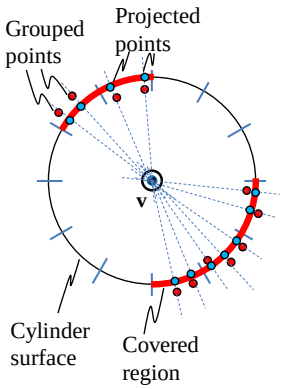

Figure 4. Point coverage of cylinder.

If the grouped points cover a small angle of the cylinder surface, the parameters of a fitted cylinder can contain aberrant values. In order to confirm whether the fitted cylinder is reliable or not, as shown in Figure 4, the cylinder surface is equiangularly divided into regions by angle θ, and scanned points are projected onto the corresponding divided cylindrical regions. If a number of regions m which contain the projected points do not satisfy $m\theta > \tau_\theta$, the points are removed from the points on pipes, where θ is $\pi/36$ and τ_θ is $\pi/2$.

5. Estimating axes and recognizing elements of a piping system

5.1 Tracing the axes of a pipeline

In the result of Section 4.2, points on elbows have been divided into several regions, and a number of cylinders are fitted to an elbow. Thus, it is difficult to estimate the true axes of elbows using the fitted cylinder axes. In order to correct the axes of these parts, axes of the piping system are traced using regions of a pipe and their pipe parameter.

As shown in Figure 5, for each pipe region, a sphere is first centered at a midpoint of axis segment s_i, where the radius of the sphere is set as 1.2 times the fitted cylinder radius r. Then, on both sides of s_i, points on the piping system $\{\mathbf{p}_k\}$ nearly existing on the sphere are collected, and a set of offset points $\{\mathbf{p'}_k\}$ is generated as $\mathbf{p}'_k = \mathbf{p}_k + r\mathbf{n}_k$, where $\mathbf{n}_k$ is a normal vector towards the inside of the pipe. Then, an average point of these offset points $\mathbf{d}$ is determined as an axis point of the pipe. These processes are repeated until points on the piping system exist on the sphere, and an axis point sequence $[\mathbf{d}_1, \mathbf{d}_2, \cdots, \mathbf{d}_n]$ is obtained for each region of the pipe.

However, in this method, as shown in Figure 6(a), when an axis point reaches a junction, only the axis point on either of the branches can be traced, and an untraced axis necessarily remains. Therefore, non-traced axes can remain. In order to recognize these untraced axes, as shown in Figure 6(b), each region is traced once again but limited to trace only the points

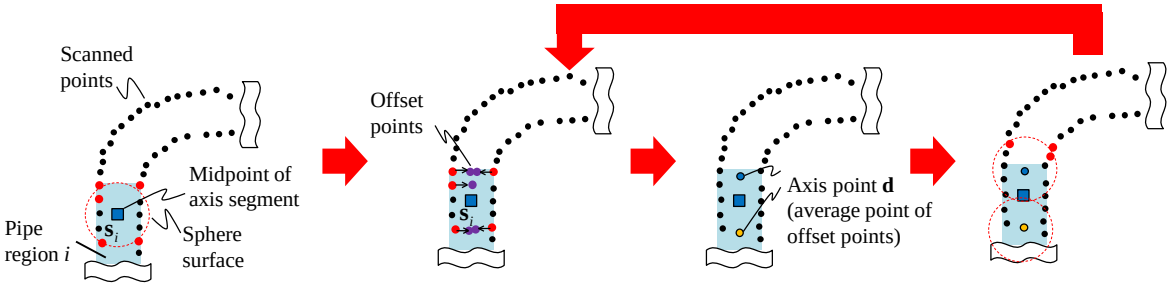

Figure 5. Tracing axes of a piping system.

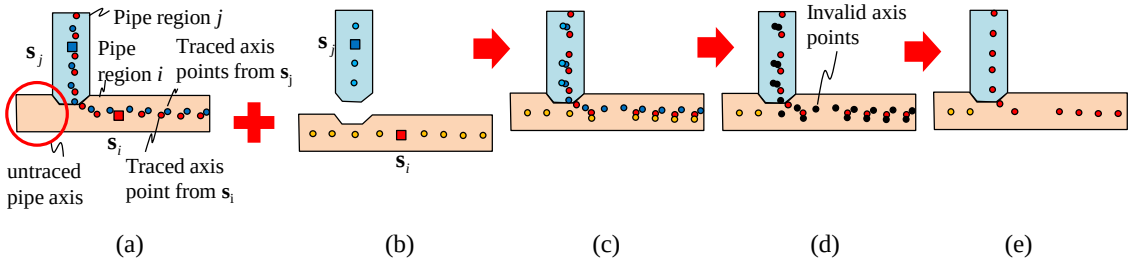

Figure 6. Tracing the axis points: (a) tracing points of all region, (b) tracing points of own region, (c) combining the two results, (d) erasing the duplicated points, (e) obtaining axis point sequences.

of their own region in the trace. After re-tracing the axes, as shown in Figure 6(c), a part of the obtained axis point sequence is duplicated. To delete these duplicated axis points, as shown in Figure 6(d), for each axis point $\mathbf{d}$, if other axis points obtained in the other steps exist in the vicinity of an axis point $\mathbf{d}$ within the distance r, these axis points are erased, as shown in Figure 6(e).

5.2 Continuous arc-line fitting

After recognizing the axis point sequence of the piping system, lines and arcs are alternatively fit to the points using a previous algorithm [15].

As shown in Figure 7, a plane Q passing three points $\mathbf{d}_i, \mathbf{d}_{i+i}, \mathbf{d}_{j+1} (i+1<j)$is first defined, and the axis points in the sequence $[\mathbf{d}_i, \cdots, \mathbf{d}_{j+1}]$ are projected onto the plane, and the projected point sub-sequence $[\mathbf{d}'_i, \cdots, \mathbf{d}'_{j+1}]$ is obtained. Next, lines $l_1 = \overline{\mathbf{d}'_i\mathbf{d}'_{i+1}}$, $l_2 = \overline{\mathbf{d}'_j\mathbf{d}'_{j+1}}$ and their intersection point $\mathbf{L}$ are calculated. Then, for each projected point $\mathbf{d}'_k \in \{\mathbf{d}'_{i+1}, \cdots, \mathbf{d}'_j\}$, a circle C, which is tangent to l_1, l_2 and $\mathbf{d}'_k$, is calculated as follows.

A tangent point $\mathbf{M}_1$ between C and l_1 satisfies equation (6):

$$R = \|\mathbf{c} - \mathbf{d}'_k\| = \|\mathbf{c} - \mathbf{M}_1\| \tag{6}$$

where $\mathbf{c}$ is a center point of C and R is a radius of C. Using the geometric relations of $\mathbf{c} = \mathbf{L} + \lambda\mathbf{t}$ and $\mathbf{M}_1 = \mathbf{d}'_i + \langle \mathbf{c} - \mathbf{d}'_i, \mathbf{v}\rangle\mathbf{v}$, where $\mathbf{t}$ is a directional vector of the bisector line of l_1 and l_2, the equation (6) can be rewritten as equations (7) and (8).

$$(\|\mathbf{w}\|^2 - \|\mathbf{t}\|^2)\lambda^2 + 2\{(\mathbf{w}\cdot\mathbf{y}) - (\mathbf{t}\cdot\mathbf{z})\}\lambda + (\|\mathbf{y}\|^2 - \|\mathbf{z}\|^2) = 0 \tag{7}$$

$$\begin{aligned}\mathbf{w} &= \mathbf{t} - (\mathbf{t}\cdot\mathbf{v})\mathbf{v}\\ \mathbf{y} &= \mathbf{L} - \mathbf{d}'_i - \{(\mathbf{L} - \mathbf{d}'_i)\cdot\mathbf{v}\}\mathbf{v}\\ \mathbf{z} &= \mathbf{L} - \mathbf{M}\end{aligned} \tag{8}$$

where $\mathbf{v}$ is a directional vector of l_1. The largest solution of the quadratic equation (7) gives the center point of $\mathbf{c}$ and the radius R of C. From the solution, a line segment $l' = \overline{\mathbf{d}'_i\mathbf{M}_1}$ and an arc segment $a' = \overline{\mathbf{M}_1\mathbf{M}_2}$ are obtained.

If any segment does not reach the last axis point $\mathbf{d}_n$, the tangent point $\mathbf{M}_2$ between C and l_2 is inserted as a new axis point, and a new line and arc segment are fitted onto the remaining axis points $[\mathbf{M}_2, \mathbf{d}'_{j+1}, \cdots, \mathbf{d}'_n]$.

However, arc segments with very large radii are sometimes fit to axis points of straight pipes. To correct these results, if

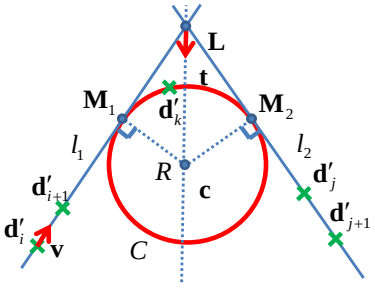

Figure 7. Arc-line fitting to an axis point sequence.

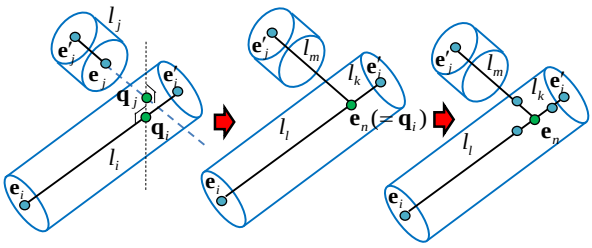

Figure 8. Interpolation of junctions.

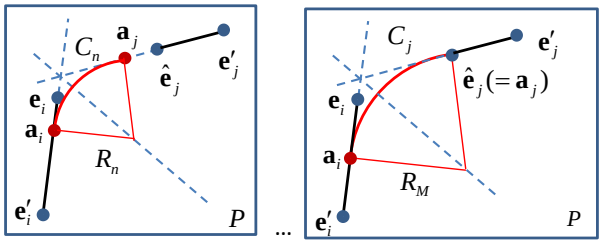

Figure 9. Interpolation of elbows.

consecutive line-arc-line segments are nearly collinear, the three segments are replaced with one line segment.

5.3 Complementing line segments on the same straight pipe

First, pairs of nearly collinear axis segments $l_i = \overline{\mathbf{e}_i\mathbf{e}_i'}$ and $l_j = \overline{\mathbf{e}_j\mathbf{e}_j'}$, which satisfy $|\mathbf{u}_i \cdot \mathbf{u}_j| > \tau_{inner}$ and $|\mathbf{u}_i \cdot \mathbf{e}_{ij}| > \tau_{inner}$, are selected, where $\mathbf{e}$ and $\mathbf{e}'$are edge points of the axis segment, $\mathbf{u}$ is a unit direction vector of the line segment, and $\mathbf{e}_{ij}$ is a unit vector of a line connecting the two edge points $\mathbf{e}_i$ and $\mathbf{e}_j$. The threshold τ_{inner} was set to be 0.98.

If the distance between $\mathbf{e}_i$ and $\mathbf{e}_j$ is less than $\boldsymbol{\tau}_l$, the two segments l_i and l_j are replaced with a new line segment $l_k = \overline{\mathbf{e}_i'\mathbf{e}_j'}$. Moreover, if any arc segment is connected with $\mathbf{e}_i$ or $\mathbf{e}_j$, a junction may be falsely recognized as an arc segment. In this case, the arc segment is removed.

5.4 Complementing line segments on the junction

After the complement of line segments on the same straight pipe, junctions that connected three pipes are identified.

As shown in Figure 8, first, a pair of line segments $l_i = \overline{\mathbf{e}_i\mathbf{e}_i'}$, $l_j = \overline{\mathbf{e}_j\mathbf{e}_j'}$, which satisfy $|\mathbf{q}_i \cdot \mathbf{q}_j| < \tau_{skew}$ and $|\mathbf{e}_i' - \mathbf{e}_i| > |\mathbf{q}_i - \mathbf{e}_i|$, are selected, where $\mathbf{q}_i$ and $\mathbf{q}_j$ are position vectors of the intersection points of the common perpendicular line of two lines L_i and L_j, which respectively passed through edge points $\mathbf{e}_i$ and $\mathbf{e}_j$, and are collinear to line axis segment l_i and l_j. τ_{skew} is a threshold for the skew distance between L_i and L_j. Then, if the segment pair gives a distance less than the pipe radius of line segment r_i, a new edge point $\mathbf{e}_n$ is placed at $\mathbf{q}_i$. Also the segments l_i and l_j are replaced with the new segments $l_k = \overline{\mathbf{e}_n\mathbf{e}_i'}$, $l_l = \overline{\mathbf{e}_n\mathbf{e}_i}$and $l_m = \overline{\mathbf{e}_n\mathbf{e}_j'}$. After the complement, the segments l_k, l_l, and l_m are respectively divided into two segments at a place of distance r' from $\mathbf{q}_i$, where r' is set as 1.1 times that of r_i. The newly divided segments which connected $\mathbf{q}_i$ are determined as a junction segment.

5.5 Complementing arc segments on the elbow

If some points on the elbow are missing due to occlusions, the axis of the elbow cannot be traced completely. In that case, an arc segment is inserted between a pair of line segments using the following steps.

First, a pair of line segments $l_i = \overline{\mathbf{e}_i\mathbf{e}_i'}$, $l_j = \overline{\mathbf{e}_j\mathbf{e}_j'}$, which satisfy $|\mathbf{q}_i \cdot \mathbf{q}_j| < \tau_{skew}$ and both distances between $\mathbf{e}_i$ and $\mathbf{q}_i$, which are less than τ_l, are selected. Then, a plane passing $\mathbf{e}_i$, $\mathbf{e}_i'$, and $\mathbf{e}_j'$ is defined, and $\mathbf{e}_j$ is projected onto the plane. A circle C_i, which is tangent to two lines L_i, L_j, and $\mathbf{e}'$, and the other circle C_j, which is tangent to L_i, L_j, and $\hat{\mathbf{e}}_j$, are calculated. L_i and L_j are lines passing l_i and l_j, and $\hat{\mathbf{e}}_j$ is the projected edge point from $\mathbf{e}_j$. By comparing the radii R_i of C_i to R_j for C_j, the larger value is adopted as the maximum value of radius R_M.

Next, as shown in Figure 9, the radius of the tangential circle C is changed step by step between 0 and R_M, and for each step, line-arc-line segments $l_{n,i} = \overline{\mathbf{a}_i\mathbf{e}_i'}$, $a_n = \overline{\mathbf{a}_i\mathbf{a}_j}$, and $l_{n,j} = \overline{\mathbf{a}_j\mathbf{e}_j'}$ are calculated. Then, two cylinder surfaces and a part of a torus surface whose axes coincide with the three segments are considered, and the distance error between scanned points and the surfaces are calculated. Finally, a combination of the segments that has the least distance error is selected.

5.6 Removing isolated axis segments

After recognizing the axes of the piping system, some non-pipe objects, such as supporting materials, are still misclassified into the piping system. To remove them, based on the connectivity, if a segment does not connect any other segments and the length of the segment is less than a threshold τ_{iso}, the segment is removed from the points of the piping system.

6. Results

6.1 Experimental results

As one of the recognition experiments, as shown in Figure 10, a large point cloud was scanned from a real oil rig by a terrestrial laser scanner (Cyra Technologies CYRAX2500). It has 4,524,324 points. The thresholds used were $r_{max} = 0.20$, $r_{min} = 0.03$, $r_1 = 0.05$, $\tau_1 = 0.30$, and $\tau_{iso} = 0.3m$. Other necessary parameter values were taken as the ones recommended in sections 3, 4 and 5.

The total recognition process took 1234.8 sec on a PC (Xeon E5520 2.27GHz), which included kd-tree construction (20.8 sec.), creating grid cells (2.7 sec.), estimating the normal vector (28.6 sec.), extracting points on a piping system

(837.1 sec.), estimating pipes on a piping system (319.5 sec.), estimating parameters of pipes (13.9 sec.), and recognizing the connection relationship (6.2 sec.).

The recognition results of the straight pipes, elbows, and junctions in the piping system are shown in Figure 10. The green cylinder expresses a straight pipe, the red torus expresses an elbow, and the blue cylinders express a junction.

The recognition accuracies of the straight pipes and the connecting parts are also summarized in Table 1. The true classes of the elements were counted by observation of the point cloud data. The recognition rate of the straight pipe was about 90%, that of the elbows was 92%, and that of junctions was 87%. Compared to the recognition rate of our former study [12], the recognition rate of straight pipes, elbows, and junctions were all improved greatly. The reason for this improvement was considered to be that by introducing the step of recognizing pipes in a piping system, almost all parts of pipes could be exhaustively extracted and recognized.

As a second example of recognition shown in Figure 11, a large point cloud was scanned from a chemical plant by a terrestrial laser scanner. It had 98,624,221 points. The thresholds used were $r_{max} = 1.25$, $r_{min} = 0.05$, $r_1 = 0.03$, $\tau_1 = 0.70$, and $\tau_{iso} = 0.30m$. The other parameter values were taken as the ones recommended in sections 3, 4, and 5.

The total recognition process took 33821.5 sec., which included kd-tree construction (751.1 sec.), creating grid cells (20.6 sec.), estimating the normal vector (618.1 sec.), extracting points on a piping system (20051.2 sec.), estimating pipes on a piping system (7952.9 sec.), estimating parameters of pipes (4332.2 sec.), and recognizing the connection relationship (4.6 sec.).

The recognition results of the straight pipes, elbows, and junctions in the piping system are shown in Figure 11. The recognition accuracies of the straight pipes and the connecting parts are also summarized in Table 2. The true classes of the elements were given by the ground truth CAD data of the plant, which had been manually modeled by a skilled operator. The recognition rate of the straight pipe was about 86%, that of elbows was 88%, and that of junctions was 71%.

6.2 Guideline of the parameters

In recognition of the piping system, five threshold values used are r_{max}, r_{min}, r_1, τ_1 and τ_{iso}. Selection criteria of these thresholds are classified into the logical criteria and trial-and-error criteria:

r_{max} and r_{min} are the maximum and minimum thresholds for the radius of recognized pipes. r_{max} should be set a bit larger from the maximum radius of the pipes in the scanned environment, and r_{min} should be set a bit lower than their minimum radius. These parameters can be set based on the estimated maximum or minimum pipe radius obtained from observing the scanned points of the piping system.

r_1 is the radius of the local search area used in region growing. r_1 should be set so that the search area includes at least one neighboring point. In our experiments, r_1 was set to include about 10 points in the search area on a pipe which had the lowest density point.

τ_1 is the threshold for the maximum distance between the endpoints of two proximal axis segments to be connected. Also, its appropriate value should be selected with trial and error.

τ_{iso} is the threshold for the maximum length of an isolated axis segment to be removed. To examine the effects of changing τ_1 and τ_{iso}, the results for the partial point clouds (440,033 points) of the oil rig are compared and shown in Figures 12 and 13 with changing $\tau_1$and τ_{iso}. The thresholds used were r_{max}=0.20, $r_{min} = 0.03$ and $r_1 = 0.05m$, and τ_1 and τ_{iso}were changed to 0.10, 0.30, and 1.50 m. The recognition rates of the straight pipes and the connecting parts are also summarized in Tables 3 and 4.

As shown in Figure 12 and Table 3, if τ_1 is selected to be much smaller than the connected pipe radius ($\tau_1 = 0.10m$), most junction parts are mis-recognized as elbow parts. To avoid these situations, it is better to set τ_1 to about at least 3-4 times the size of the connected pipe radius. In contrast, if τ_1 becomes larger than that ($\tau_1 = 1.50m$), some false pairs of segments are connected. It is difficult to find a maximum range of $\tau_1$because it greatly depends on the range of the occluded regions and the structure of the piping system. Therefore, so far, τ_1 has been set with trial and error.

On the other hand, as shown in Figure 13 and Table 4, if τ_{iso} is selected to be too small ($\tau_1 = 0.10m$), some non-pipe objects still remain as pipes. In contrast, if τ_{iso} becomes too large ($\tau_1 = 1.50m$), some isolated straight pipes disappear. Unfortunately, it is difficult to find the optimal value of τ_{iso} in an *a priori* manner, because it greatly depends on the structure of the piping system. Therefore, so far, τ_{iso} is set with trial and error manner. However, as shown in the recognition results of the experiment, the setting of τ_{iso} is not necessarily strict. τ_{iso} can be set to any value less than the length where straight pipes can be distinguish from non-pipe objects. The results of the experiment showed that τ_{iso} did not affect the recognition rates of the piping system much, if this condition is satisfied.

6.3 Discussion

In these results, the lowest recognition rates of the straight pipes, elbows, and junctions were about 86%, 88%, and 71% respectively.

The recognition rates of the related work [6] were 97%, 100%, and 86%. However, their input point clouds only consisted of a cloud on the pipes, and the amount, density, and complexity of the piping objects were much smaller than ours. On the other hand [16, 17], the recognition rates of the cylindrical surface of industrial tools and commodities range from 75% to 90%. Considering the complexity of the input point clouds, our recognition rates were considered to be appropriate.

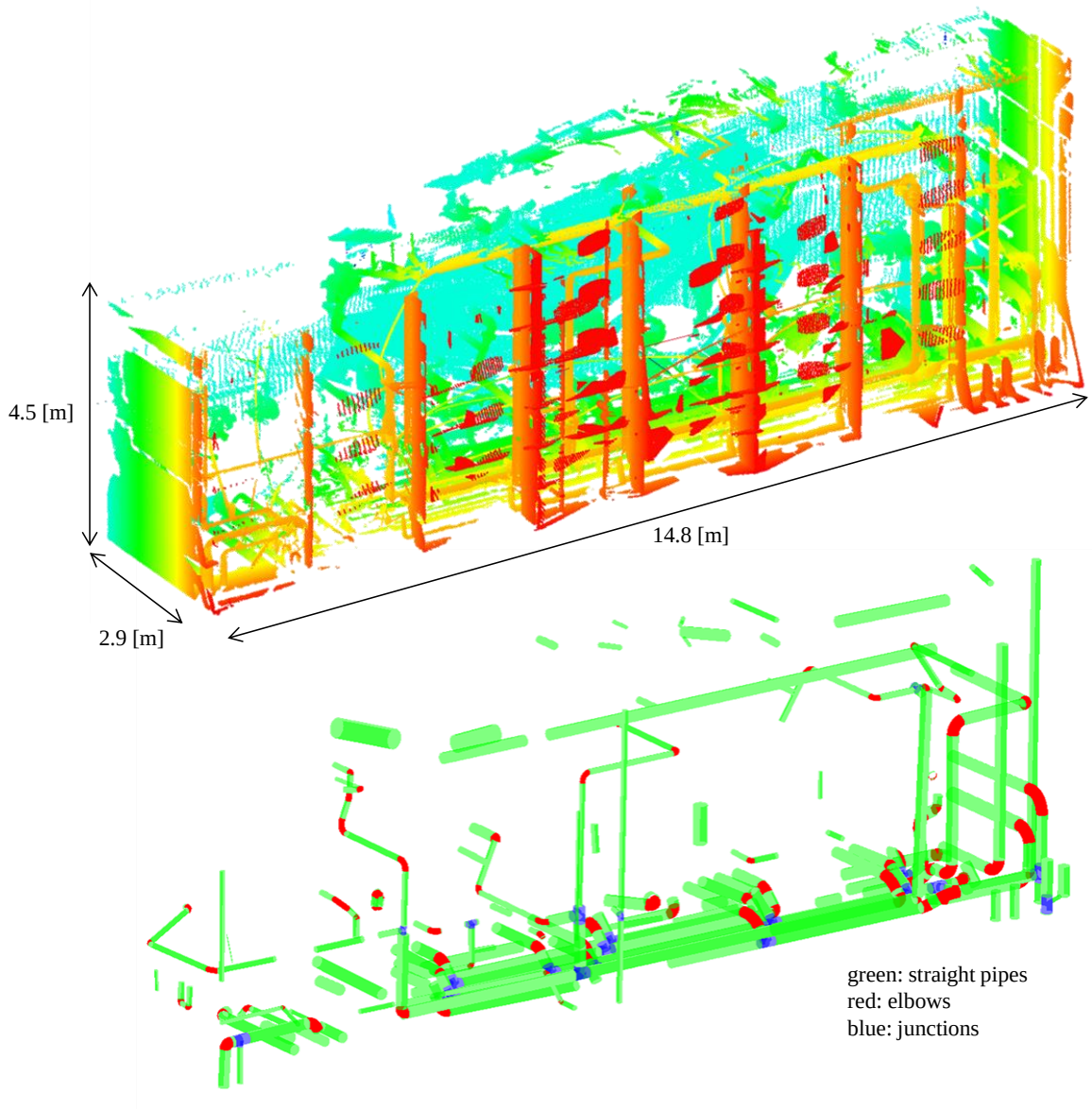

Figure 10. The original scanned points (upper) and the recognition result of the piping system (lower) of an oil rig.

Table 1. Accuracy of the piping system recognition of an oil rig.

(a) Pipe

		Result of Automatic Recognition				False Recognition	
		Pipe	Not Recognized	Total	Recognition rate [%]	False Negative [%]	False Positive [%]
True class	Pipe	130	13	143	90.9	9.1	37.1
	Other	77	-	-	-	-	-
	Total	207	-	-	-	-	-

(b) Connecting parts

		Result of Automatic Recognition					False Recognition	
		Elbow	Junction	Not Recognized	Total	Recognition Rate [%]	False Negative [%]	False Positive [%]
True class	Elbow	65	0	5	70	92.8	7.2	21.4
	Junction	1	20	2	23	87.0	13.0	13.0
	Others	16	3	-	-	-	-	-
	Total	84	23	-	-	-	-	-

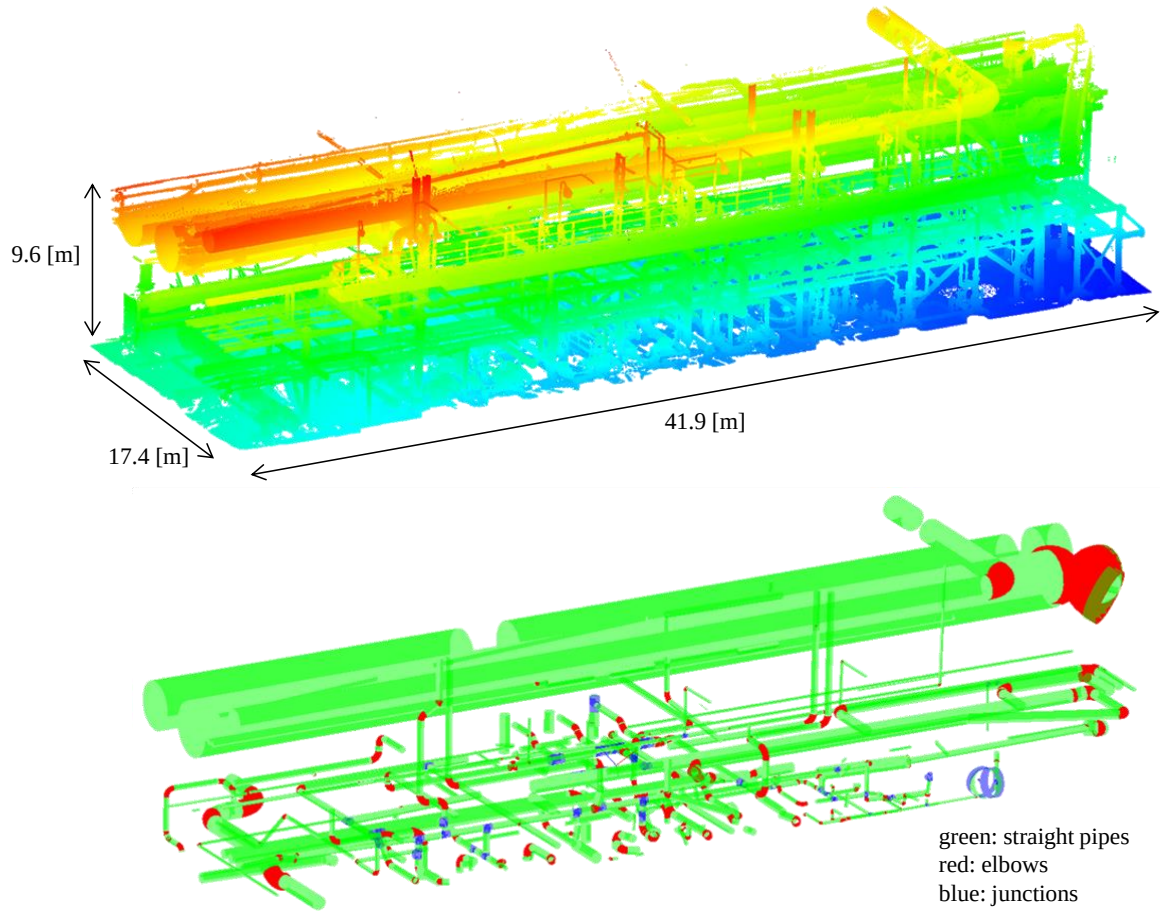

Figure 11. The original scanned points (upper) and the recognition result of the piping system (lower) of a chemical plant.

Table 2. Accuracy of the piping system recognition of a chemical plant.

(a) Pipe

		Result of Automatic Recognition				False Recognition	
		Pipe	Not Recognized	Total	Recognition Rate [%]	False Negative [%]	False Positive [%]
True Class	Pipe	159	24	183	86.9	13.1	62.7
	Other	267	-	-	-	-	-
	Total	426	-	-	-	-	-

(b) Connecting parts

		Result of Automatic Recognition					False Recognition	
		Elbow	Junction	Not Recognized	Total	Recognition Rate [%]	False Negative [%]	False Positive [%]
True Class	Elbow	80	0	10	90	88.9	11.1	62.4
	Junction	5	20	3	28	71.4	28.6	51.2
	Others	126	21	-	-	-	-	-
	Total	211	41	-	-	-	-	-

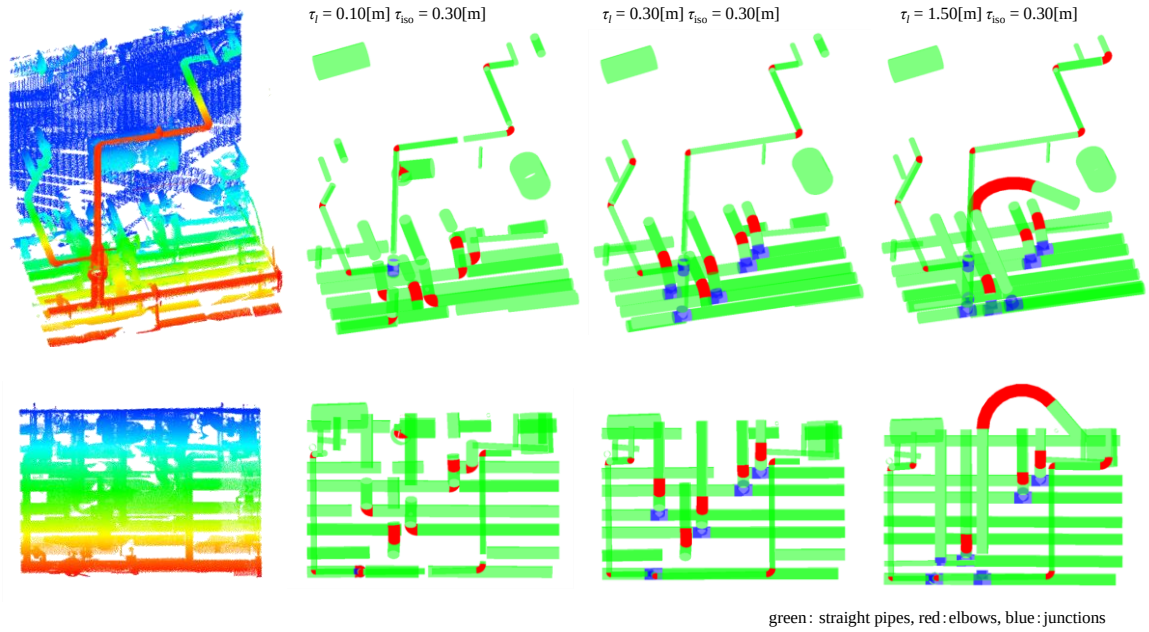

Figure 12. A part of the original scanned points (left) and the recognition results of the piping system (right) of an oil rig.

Table 3. Accuracy of the piping system recognition of an oil rig.

(a) Pipe

τ_l = 0.10[m] τ_{iso} = 0.30[m]

		Result of Automatic Recognition				False Recognition	
		Pipe	Not Recognized	Total	Recognition Rate [%]	False Negative [%]	False Positive [%]
True Class	Pipe	24	10	34	70.6	29.5	56.4
	Other	10	-	-	-	-	-
	Total	55	-	-	-	-	-

τ_l = 0.30[m] τ_{iso} = 0.30[m]

		Result of automatic recognition				False recognition	
		Pipe	Not recognized	Total	Recognition rate [%]	False negative [%]	False positive [%]
True Class	Pipe	32	2	34	94.1	5.9	28.9
	Other	13	-	-	-	-	-
	Total	45	-	-	-	-	-

τ_l = 1.50[m] τ_{iso} = 0.30[m]

		Result of Automatic Recognition				False Recognition	
		Pipe	Not Recognized	Total	Recognition Rate [%]	False Negative [%]	False Positive [%]
True Class	Pipe	23	11	34	67.6	32.4	45.2
	Other	19	-	-	-	-	-
	Total	42	-	-	-	-	-

(b) Connecting parts

		Result of Automatic Recognition					False Recognition	
		Elbow	Junction	Not Recognized	Total	Recognition Rate [%]	False Negative [%]	False Positive [%]
True Class	Elbow	7	0	5	12	58.3	41.7	50.0
	Junction	5	1	1	7	14.3	84.7	0.0
	Others	2	0	-	-	-	-	-
	Total	14	1	-	-	-	-	-

		Result of Automatic Recognition					False Recognition	
		Elbow	Junction	Not Recognized	Total	Recognition Rate [%]	False Negative [%]	False Positive [%]
True Class	Elbow	11	0	1	912	91.7	8.3	0.0
	Junction	0	6	1	7	85.7	14.3	0.0
	Others	0	0	-	-	-	-	-
	Total	11	6	-	-	-	-	-

		Result of automatic recognition					False recognition	
		Elbow	Junction	Not Recognized	Total	Recognition Rate [%]	False Negative [%]	False Positive [%]
True Class	Elbow	10	0	2	12	83.3	16.7	9.1
	Junction	0	5	2	7	71.4	28.6	28.6
	Others	1	2	-	-	-	-	-
	Total	11	7	-	-	-	-	-

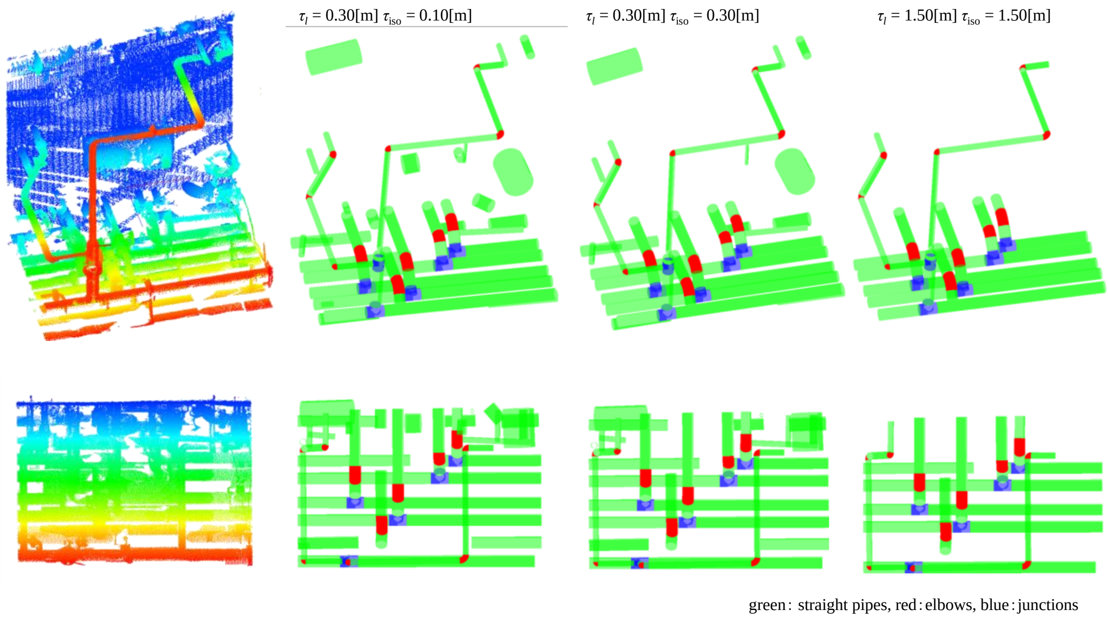

Figure 13. A part of the original scanned points (left) and the recognition results of the piping system (right) of an oil rig.

Table 4. Accuracy of the piping system recognition of an oil rig.

(a) Pipe

τ_l = 0.30[m] τ_{iso} = 0.10[m]

		Result of Automatic Recognition				False Recognition	
		Pipe	Not Recognized	Total	Recognition Rate [%]	False Negative [%]	False Positive [%]
True Class	Pipe	32	2	34	94.1	5.9	37.6
	Other	19	-	-	-	-	-
	Total	51	-	-	-	-	-

τ_l = 0.30[m] τ_{iso} = 0.30[m]

		Result of Automatic Recognition				False Recognition	
		Pipe	Not Recognized	Total	Recognition Rate [%]	False Negative [%]	False Positive [%]
True Class	Pipe	32	2	34	94.1	5.9	28.9
	Other	13	-	-	-	-	-
	Total	45	-	-	-	-	-

τ_l = 0.30[m] τ_{iso} = 1.50[m]

		Result of Automatic Recognition				False Recognition	
		Pipe	Not Recognized	Total	Recognition Rate [%]	False Negative [%]	False Positive [%]
True Class	Pipe	28	6	34	82.3	17.7	0.0
	Other	0	-	-	-	-	-
	Total	28	-	-	-	-	-

(b) Connecting parts

		Result of Automatic Recognition					False Recognition	
		Elbow	Junction	Not Recognized	Total	Recognition Rate [%]	False Negative [%]	False Positive [%]
True Class	Elbow	11	0	1	12	91.7	8.3	0.0
	Junction	0	6	1	7	85.7	14.3	0.0
	Others	0	0	-	-	-	-	-
	Total	11	6	-	-	-	-	-

		Result of Automatic Recognition					False Recognition	
		Elbow	Junction	Not Recognized	Total	Recognition Rate [%]	False Negative [%]	False Positive [%]
True Class	Elbow	11	0	1	12	91.7	8.3	0.0
	Junction	0	6	1	7	85.7	14.3	0.0
	Others	0	0	-	-	-	-	-
	Total	11	6	-	-	-	-	-

		Result of Automatic Recognition					False Recognition	
		Elbow	Junction	Not Recognized	Total	Recognition Rate [%]	False Negative [%]	False Positive [%]
True Class	Elbow	11	0	1	12	91.7	8.3	0.0
	Junction	0	6	1	7	85.7	14.3	0.0
	Others	0	0	-	-	-	-	-
	Total	11	6	-	-	-	-	-

If there is any pipe with a large radius, the range of the pipe radius to be recognized increases. Therefore, non-pipe objects which are misrecognized as pipes increase. These mis-recognized objects can be connected to other true pipes in the step of complementing segments of straight, junction, and elbow parts. Therefore, the accuracy of the piping system recognition becomes worse. For this reason, the accuracy of the recognition of the chemical plant became lower than that of the oil rig in our results.

Also, in both of these results, false positive recognition in straight pipes, junctions, and elbows was not uncommon. This was because the partial shape of some non-pipe objects, such as H-beams, had a similar shape to that of a cylinder, and those parts were misrecognized as pipes.

These two problems can be reduced by cross-sectional analysis. This is left for future work.

7. Conclusions

A new algorithm was proposed that could automatically recognize a piping system from registered laser-scanned points of a plant. Normal-based region growing allows one to exhaustively extract the points on a piping system and to segment the points of each pipe. Cylinder fitting could extract only the point, including straight pipes, elbows, and junctions. Tracing axes, fitting arc-line segments, and the complementing of segments could recognize the position of straight pipes, elbows, and junctions and their connection relationship.

The recognition accuracy was verified for large-scale point clouds of actual plants, and the results showed the recognition rate of the straight pipes, elbows, and junctions exceeded 86%, 88%, and 71% respectively, and the effectiveness of the proposed algorithm for the reverse engineering of the plants was clarified.

However, the recognition accuracy of junction parts was low. Also, false positive recognition was not uncommon. The improvement of this accuracy is left for future work.

Acknowledgments

We wish to thank the Research Institute for Science and Engineering, Leica Co., Ltd and Sanki Co., Ltd for providing the laser-scanned data sets. This research was financially supported by the Japan Ministry of Education, Culture, Sports, Science, and Technology Grant-in-Aid for Scientific Research (B) under the project No. 24360057.

References

[1] Masuda H, Tanaka I, Enomoto M. Reliable surface extraction from point-clouds using scanner-dependent parameters. Computer-Aided Design and Applications. 2012; 10(2): 265-277.

[2] Rabbani T, Heuvel F. 3d industrial reconstruction by fitting CSG models to a combination of images and point clouds. In: Proceeings of ISPRS The International Archives of Photogrammetry, Remote Sensing and Spatial Information Sciences; 2004 July 12-23; IST, Turkey; 35(B3): p.7-12.

[3] Aurelien B, Chaine R, Marc R, Thibault G, Akkouche S. Reconstruction of consistent 3d CAD models from point cloud data using a priori CAD models. In: ISPRS Workshop Laser Scanning 2011; 2011 Aug 29-31; Calgary, Canada; submission-26.

[4] Johnson A, Hoffman R, Osborn J, Hebert M. A system for semi-automatic modeling of complex environments. In: Proceedings of IEEE International Conference on Recent Advances in 3-D Digital Imaging and Modeling; 1997 May 12-15; Ottawa, Canada; p.213-220.

[5] Namatame T, Mizoguti T, Kobayashi Y, Shirai K. As-build modeling using Manhattan-world assumption(in Japanese). In: Proceedings of the 2011 Japan Society for Precision Engineering Autumn meeting; 2011 Sep 20-22; Kanazawa, Japan; F06.

[6] Lee J, Kim C, Son H, Kim C. Skeleton-based 3d reconstruction of as-built pipelines from laser-scanned data. In: Proceedings of the 2012 ASCE International Conference on Computing in Civil Engineering; 2012 Jun 17-20; Clearwater Beach, FL: p.245-252.

[7] Belton D, Lichti D. Classification and segmentation of terrestrial laserscanner point clouds using local variance information. International Archives of the Photogrammetry, Remote Sensing and Spatial Information Sciences. 2006; 36(5): 44-49.

[8] Rabbani T, Heuvel F, Vosselman G. Segmentation of point clouds using smoothness constraint. International Archives of the Photogrammetry, Remote Sensing and Spatial Information Sciences. 2006; 36: 248-253.

[9] Vosselman G, Gorte BGH, Sithole G, Rabbani T. Recognising structure in laser scanner point clouds. International Archives of Photogrammetry, Remote Sensing and Spatial Information Sciences. 2004; 46: 33-38.

[10] El-Halawany S, Lichti D. Detection of road poles from mobile terrestrial laser scanner point cloud. In: C2011 International Workshop on Multi-Platform/MultiSensor Remote Sensing and Mapping (M2RSM); 2011 Jan 10-12; Xiamen, China; p.1-6.

[11] Marshall AD, Lukacs G, Martin RR. Robust segmentation of primitives from range data in the presence of geometric degeneracy. IEEE Transactions on Pattern Analysis and Machine Intelligence. 2001; 23(3): 304-314.

[12] Kawashima K, Kanai S, Date H. Automatic recognition and modeling of piping system from large-scale terrestrial laser scanned point cloud. In: 2012 Asian Conference on Design and Digital Engineering; 2012 Dec 6-8; Niseko, Japan; 100022.

[13] Maronna RA, Martin DR, Yohai VJ. Robust statistics: theory and methods. Chichester (UK): John Wiley & Sons, Ltd.; 2006. 436 p.

[14] Shakarji MC. Least-squares fitting algorithms of the NIST

algorithm testing system. Journal of Research of the National Institute of Standards and Technology. 1998; 103(6): 633-641.

[15] Bauer U, Polthier K. Generating parametric models of tubes from laser scans. Computer-Aided Design. 2009; 41(10): 719-729.

[16] Rusu RB, Martin ZC, Beetz M. Learning informative point classes for the acquisition of object model maps. In: Proceedings of International Conference on Control, Automation, Robotics and Vision; 2008 Dec 17-20; Hanoi, Vietnam; p.643-650.

[17] Biegelbauer G, Vincze M. Efficient 3d object detection by fitting superquadrics to range image data for robot's object manipulation. In: Proceedings of IEEE International Conference on Robotics and Automation; 2007 Apr 10-14; Roma, Italy; p.1086-1091.